Received: 18 April 2022 | Revised: 28 June 2022 | Accepted: 14 July 2022

DOI: 10.1002/dug2.12013

RESEARCH ARTICLE

DUSE WILEY

Frictional stability of Longmaxi shale gouges and its implication for deep seismic potential in the southeastern Sichuan Basin

Fengshou Zhang[1,2] | **Li Cui**[1,2] | **Mengke An**[1,2] | **Derek Elsworth**[3,4] | **Changrong He**[5]

[1]Department of Geotechnical Engineering, College of Civil Engineering, Tongji University, Shanghai, China

[2]Key Laboratory of Geotechnical and Underground Engineering of Ministry of Education, Tongji University, Shanghai, China

[3]Department of Energy and Mineral Engineering, EMS Energy Institute and G3 Center, The Pennsylvania State University, State College, Pennsylvania, USA

[4]Department of Geosciences, The Pennsylvania State University, State College, Pennsylvania, USA

[5]State Key Laboratory of Earthquake Dynamics, Institute of Geology, China Earthquake Administration, Beijing, China

Correspondence

Mengke An, Department of Geotechnical Engineering, College of Civil Engineering, Tongji University, 200092 Shanghai, China.
Email: 2015mengkean@tongji.edu.cn

Funding information

Fundamental Research Funds for the Central Universities; China Postdoctoral Science Foundation, Grant/Award Numbers: 2021M692448, 2022T150483; National Natural Science Foundation of China, Grant/Award Numbers: 42077247, 42107163

Abstract

Microearthquakes accompanying shale gas recovery highlight the importance of exploring the frictional and stability properties of shale gouges. Aiming to reveal the influencing factors on fault stability, this paper explores the impact of mineral compositions, effective stress and temperature on the frictional stability of Longmaxi shale gouges in deep reservoirs located in the Luzhou area, southeastern Sichuan Basin. Eleven shear experiments were conducted to define the frictional strength and stability of five shale gouges. The specific experimental conditions were as follows: temperatures: 90–270°C; a confining stress: 95 MPa; and pore fluid pressures: 25–55 MPa. The results show that all five shale gouges generally display high frictional strength with friction coefficients ranging from 0.60 to 0.70 at the aforementioned experiment condition of pressures, and temperatures. Frictional stability is significantly affected by temperature and mineral compositions, but is insensitive to variation in pore fluid pressures. Fault instability is enhanced at higher temperatures (especially at >200°C) and with higher tectosilicate/carbonate contents. The results demonstrate that the combined effect of mineral composition and temperature is particularly important for induced seismicity during hydraulic fracturing in deep shale reservoirs.

KEYWORDS

deep shale reservoir, hydraulic fracturing, hydrothermal condition, induced seismicity, mineral composition, shale fault stability

1 | INTRODUCTION

In recent years, induced earthquakes resulting from unconventional resource extraction activities have attracted growing public attention. Such activities include hydraulic fracturing for shale gas exploitation, wastewater injection, and CO_2 geological sequestration (Atkinson et al., 2020; Bao & Eaton, 2016; Cappa & Rutqvist, 2011; Clarke et al., 2019; Elsworth et al., 2016; Juanes et al., 2016). Several moderate to large earthquakes have been shown to be a threat to society. For example, the M_L 5.7 earthquake on December 16, 2018 in southwest China related to shale gas exploitation by hydraulic fracturing has resulted in significant losses (Lei et al., 2019b). The Mw 5.5 earthquake that occurred on November 15, 2017 in Pohang of South Korea was known as the largest induced earthquake related to enhanced geothermal systems (EGS) in the world (Grigoli et al., 2018). In addition, induced earthquakes mainly associated with EGS and deep injection of wastewater occurred in Basel (Grigoli et al., 2017), Oklahoma and Arkansas (Ellsworth, 2013), and Texas (Schultz et al., 2020) as well. All of these show a clear correlation between induced seismicity with fluid

injection and highlight the importance of understanding the underlying mechanisms of the reactivation of pre-existing faults/fractures (Candela et al., 2018; Lei et al., 2019a; Verdon & Bommer, 2020).

The Sichuan Basin (Figure 1a) of China is rich in shale gas resources and has optimistic prospects for development (C. Zou et al., 2015). However, the number of earthquakes in this area has increased sharply since the initiation of hydraulic fracturing for shale gas exploitation and recovery (An, Zhang, Elsworth, et al., 2020) in 2011, principally due to hydraulic fracturing, especially in the Changning and Weiyuan areas (Ma, 2018). Meanwhile, multiple earthquakes with $Mw > 4$ have been reported, including the Mw 4.7 earthquake in the Changning block on January 27, 2017, 9 days after hydraulic fracturing (Lei et al., 2017), the Mw 4.8 earthquake in the Changning block on January 3, 2019, and the Mw 4.9 earthquake in the Weiyuan block on September 7, 2019 (Lei et al., 2019b). These induced seismic events have resulted in important socioeconomic impacts. All these events were demonstrated to be highly correlated to hydraulic fracturing. At present, the shale gas recovery in the Sichuan Basin is still in the developing stages and the main target shale reservoirs are generally located at depths <3.5 km. With the increase in reservoir depth in the southeastern Sichuan Basin, both the shale compositions and the geologic environments have significantly changed. In this sense, exploring the frictional and stability properties of the deep Longmaxi shale faults under hydrothermal conditions is of great significance in providing an insight into understanding the mechanisms of induced seismicity during hydraulic fracturing and subsequent production of the deep shale reservoirs. This research offers a basis for better choices in production safety and risk mitigation.

Frictional and stability properties of shale faults at shallow depth have been extensively studied in recent years (Fang et al., 2017; Guglielmi et al., 2015; Jia et al., 2019; Scuderi & Collettini, 2018; F. Zhang et al., 2017, 2019). Evidently, as is shown by the results of previous related studies, the frictional properties of the pre-existing fault or fracture exert some significant controls on its reactivation, especially the mineral compositions, temperatures, and applied stresses (Fang et al., 2016; Scuderi & Collettini, 2016; Segall & Lu, 2015; Yasuhara et al., 2004). In terms of mineralogy, the contents of phyllosilicate minerals play an important role in fault stability (An, Zhang, Elsworth, et al., 2020; Fang et al., 2018; L. Zhang & He, 2016), and faults with less phyllosilicates are prone to exhibit unstable slips (Kohli & Zoback, 2013). The high temperature not only changes the gouge composition through chemical reactions but also accelerates fluid-assisted stages including pressure dissolution (Yasuhara et al., 2005). In addition, the change in effective stress was generally associated with the change in pore pressure caused by fluid injection. A higher pore fluid pressure often leads to reduced effective stress on pre-existing faults, thus resulting in fault instability (Candela et al., 2015; Elsworth et al., 2016). Considering the frequent fluid injection in the southern Sichuan Basin and the ambiguous mechanisms of induced earthquakes in Longmaxi shales, it is particularly important to explore the parameters controlling the instability of deep shale faults (López-Comino & Cesca, 2018).

The first-order trends were defined in the mineral composition of the Longmaxi shale in the southeastern Sichuan Basin. Based on the data on these compositions, tri-axial shear experiments were conducted at high temperatures (90–270°C) and high fluid pressures

FIGURE 1 The location of the research region and the shale samples. (a) The research region of Sichuan Basin. (b) Luzhou area and Weiyuan area in the southeastern Sichuan Basin (Lei et al., 2020). (c) The sketch plots of the collected five shale samples.

(25–55 MPa) to study the evolution of friction and stability in the simulated Longmaxi shale gouges. The geological background of the southeastern Sichuan Basin and the existing record of induced earthquakes (Chang et al., 2020) were combined to define the coupled influences of the mineral composition, effective stress and temperature on the clusters of earthquakes in the Longmaxi formation due to hydraulic fracturing.

2 | EXPERIMENTAL METHODS

2.1 | Gouge preparations

Five samples of the deep Longmaxi shales were collected from rock core cuttings in the southeastern Sichuan Basin. All samples (Figure 1c) were recovered from boreholes with depths > 3700 m in the Luzhou block (Figure 1b). After removing the surface impurities, all shales were crushed through a pestle and mortar and then sieved to a grain diameter < 74 μm to simulate comminuted fault gouge. The mineral compositions of the five samples were tested by X-ray diffraction method and the results are shown in Table 1. Abundant minerals in Longmaxi shales include quartz, plagioclase, calcite, dolomite, and clay minerals with a trace of pyrite. With an increase in depth, the quartz content first increases and then decreases, while the total clay content displays the opposite trend. The highest quartz content in the studied shales reaches 68 wt.%, and the minimum is only 26 wt.%. The total clay content ranges from 5 to 38 wt.% (Table 1). The mineral composition of the Longmaxi shale samples is characterized by an increase in tectosilicate contents.

2.2 | Apparatus and testing procedure

The shear experiments on simulated gouges were completed in an argon-gas-confined high-temperature and high-pressure tri-axial shear apparatus (Figure 2) at the Institute of Geology, China Earthquake Administration, Beijing, China. The maximum temperature for the apparatus is 600°C, the maximum confining pressure is 420 MPa, and the maximum pore fluid pressure is 200 MPa. A 1-mm-thick gouge layer was emplaced between the upper and lower forcing blocks of saw-cut cylinders (20 mm in diameter; 40 mm in height) and at an inclination of 35°. Two perpendicular holes were drilled in the upper forcing block as a channel for pore fluid entry. The porous brass filter was inserted into the two boreholes to prevent gouge extrusion while maintaining a high permeability of pore fluid. The gouge thickness was guaranteed by a specially made cylindrical leveling jig. Once filled with a layer of gouge, the gabbro block was inserted into a copper jacket with a thickness of 0.35 mm, followed by placing the cylindrical tungsten–carbide and corundum blocks on both sides. The boron nitride powder was adopted to fill the space between the copper tube and the heating furnace to prevent gas convection. Two

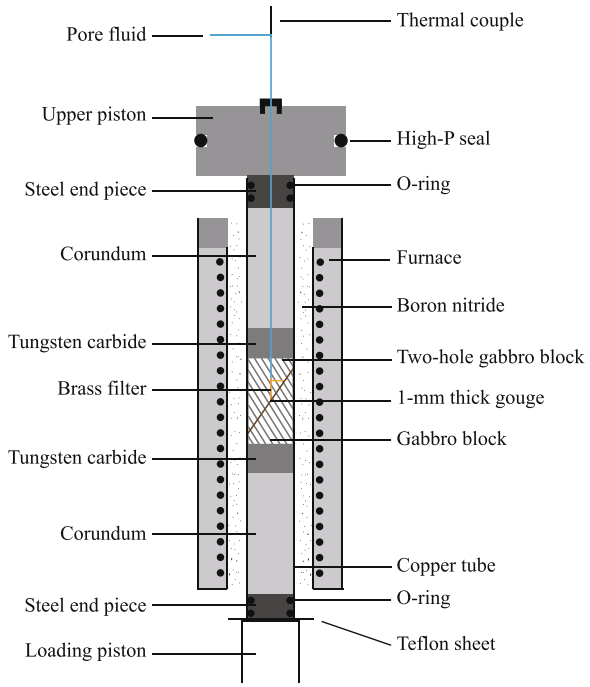

FIGURE 2 Schematic of the tri-axial shear apparatus

TABLE 1 Mineral compositions of the collected Longmaxi shales

Shales	SSC3730-1	SSC3730-2	SSC3740-1	SSC3740-2	SSC3750
Recovered depth (m)	3730	3730	3740	3740	3750
Quartz (%)	46	56	68	65	26
Plagioclase (%)	9	5	4	3	10
Calcite (%)	4	4	12	3	17
Dolomite (%)	5	4	9	22	9
Pyrite (%)	4	7	2	2	-
Illite (%)	24	17	4	3	35
Chlorite (%)	5	4	-	1	-
Others (%)	3	3	1	1	3
Total clay (%)	29	21	4	3	35

Note: The clay minerals mainly include illite and chlorite (%).

O-rings were placed on the steel end blocks on either side of the copper tube to isolate samples from the argon gas. The high-pressure seal on the upper piston could prevent the gas from escaping from the pressure vessel and thus seal the whole experimental system.

The experimental procedures are as follows: First, the confining and pore fluid pressures were raised to 70%–80% of the target values. Then, the temperature was raised to the target value at a heating rate of 5°C/min. A thermocouple was installed at the pore fluid inlet to measure the temperature. The temperature was maintained constant within ±2°C by an independent controller during the experiments. When the temperature was raised to the desired value, the confining and pore fluid pressures were elevated to the target values and remained stable within ±0.5 and ±0.3 MPa by the servo control system. At the beginning of each experiment, the sample was loaded at a constant axial shear velocity of 1.0 μm/s. Once the steady state of friction was achieved, the axial shear velocity first declined and then increased, following the sequence of 1–0.2–0.04–0.2–1–0.2–0.04 μm/s, equivalent to the velocities along the shear direction switching between 1.22, 0.244, 0.0488, 0.244, 1.22, 0.244, and 0.0488 μm/s successively. The final shear displacements were generally within the range of 3–4 mm.

In total, 11 experiments were performed at different temperatures and pressures and the experiment details are shown in Table 2. Five experiments (testing nos.: SSC3730-1-130, SSC3730-2-130, SSC3740-1-130, SSC3740-2-130, and SSC3750-130) were completed under a confining pressure (σ_c) of 95 MPa, a pore fluid pressure (P_f) of 40 MPa, and a temperature (T) of 130°C to explore the frictional properties of the shale gouges at in situ hydrothermal conditions. In addition, three experiments (testing nos.: SSC3730-1-90, SSC3730-1-200, and SSC3730-270) were conducted at temperatures of 90–270°C on sample SSC3730-1 to define the temperature dependence (X. Zou et al., 2022), and another three experiments (testing nos.: SSC3740-2-25, SSC3740-2-40, and SSC3740-2-55) were carried out at pore fluid pressures of 25–55 MPa on sample SSC3740-2, to probe the effect of the variation in pore fluid pressure.

2.3 | Data analysis

In the experiments, the raw data including the axial load, pore fluid pressure, temperature, and axial displacement at a sampling frequency of 1 Hz were recorded. The raw data were corrected according to the method proposed by He et al. (2006) to incorporate the influences caused by the change in contact area with increasing displacement and the shear resistance of the copper tube. The frictional strength of the studied gouges was determined by the frictional coefficient μ, which could be calculated from shear stress τ divided by effective normal stress σ_{neff} (ignoring the cohesion), shown as follows:

$$\mu = \frac{\tau}{\sigma_{neff}} = \frac{\tau}{(\sigma_n - Pp_f)}, \quad (1)$$

where σ_n represents the applied normal stress and p_f denotes the applied pore fluid pressure.

The velocity dependence of friction $(a-b)$ can be explained according to the rate- and state-friction (RSF) constitutive theory (Dieterich, 1978, 1979; Marone, 1998; Ruina, 1983). In the category of RSF theory, the frictional coefficient μ is calculated as

$$\mu = \mu_0 + a\ln\left(\frac{V}{V_0}\right) + b\ln\left(\frac{V_0\theta}{D_c}\right), \quad (2)$$

$$\frac{d\theta}{dt} = 1 - \frac{V\theta}{D_c}, \quad (3)$$

where μ is the coefficient of friction at the instantaneous shear velocity V, μ_0 denotes the coefficient of friction at the reference velocity V_0, θ represents a state variable, a and b refer to the frictional parameters representing the direct and evolutional effects caused by the step change

TABLE 2 Experimental conditions

Tests	Samples	σ_c (MPa)	P_f (MPa)	T (°C)	l_{final} (mm)	Frictional responses
SSC3730-1-90	SSC3730-1	95	40	90	3.38	vs
SSC3730-1-130	SSC3730-1	95	40	130	2.97	vs
SSC3730-1-200	SSC3730-1	95	40	200	3.34	vs
SSC3730-1-270	SSC3730-1	95	40	270	3.58	Mixed; vw, ss
SSC3730-2-130	SSC3730-2	95	40	130	3.30	vs
SSC3740-1-130	SSC3740-1	95	40	130	3.09	vs
SSC3740-2-25	SSC3740-2	95	25	200	3.63	Mixed; vs, vw
SSC3740-2-130	SSC3740-2	95	40	130	3.27	vs
SSC3740-2-40	SSC3740-2	95	40	200	3.58	vw
SSC3740-2-55	SSC3740-2	95	55	200	3.45	vw
SSC3750-130	SSC3750	95	40	130	3.22	vs

Abbreviations: σ_c, confining pressure; l_{final}, final shear displacement; P_f, pore fluid pressure; ss, stick-slip; T, temperature; vs, velocity-strengthening; vw, velocity-weakening.

of shear velocity, respectively, and D_c denotes the critical slip distance from the past steady state to a new steady state. In a steady state of friction, the velocity dependence $(a-b)$ is calculated as

$$a-b=\frac{\mu-\mu_0}{\ln\left(\frac{V}{V_0}\right)}. \tag{4}$$

The positive value of $(a-b)$ indicates velocity-strengthening behavior under a velocity step (Figure 3a) and generally promotes stable fault sliding. Conversely, a negative value of $(a-b)$ represents velocity-weakening behavior, and unstable sliding occurs whenever the critical stiffness is satisfied (Figure 3a). When the gouges show stick-slip behavior, the method for calculation of $(a-b)$ is as shown in Figure 3b. In addition, the slope was also detrended in calculating the $(a-b)$ values following the methods in Figure 3c.

3 | RESULTS

3.1 | Impact of mineral composition on shale gouge friction

By using the method in Section 2.3, five shear experiments on different shale gouges were conducted under experimental conditions of $\sigma_c = 95$ MPa, $p = 40$ MPa, and $T = 130$°C, with the coefficient of friction–shear displacement curves shown in Figures 4 and 6b. In the first ~0.5 mm of shear displacement, each gouge displayed a linear increase in friction until approaching a steady state. After a shear displacement of ~1.0 mm, all gouges showed a strain-hardening response. The steady-state frictional coefficients were evaluated at a shear displacement of approximately ~2.5 mm and a shear velocity of 1.22 μm/s and the results are shown in Figure 5a. The frictional coefficient μ of the five shale gouges was in the range of ~0.55–0.7, consistent with those of previous studies on shale gouges with similar phyllosilicate contents (Kohli & Zoback, 2013). A higher frictional coefficient in shale gouge SSC3740-2 was possibly due to a higher carbonate content (~25 wt.%) and a lower phyllosilicate content (~5 wt.%) (Figure 5a and Table 1). Conversely, the shale gouge SSC3750 showed the lowest coefficient of friction (~0.57) and this possibly resulted from its highest phyllosilicate content (38 wt.%). By using the methods in Section 2.3, frictional stability $(a-b)$ was calculated and the results are presented in Figure 5b. Values of $(a-b)$ for the five shale gouges were in the range of ~0.001–0.008, suggesting that all shales were prone to contribute to a stable fault slip (Figure 5b and Table 3). Meanwhile, there existed a clear correlation between the frictional stability $(a-b)$ and the phyllosilicate content and this phenomenon is in accord with the results of Ikari et al. (2011).

3.2 | Impact of temperature on shale gouge friction

To explore the temperature dependence of frictional coefficient and stability, four shear experiments were conducted on shale gouge SSC3730-1 under the

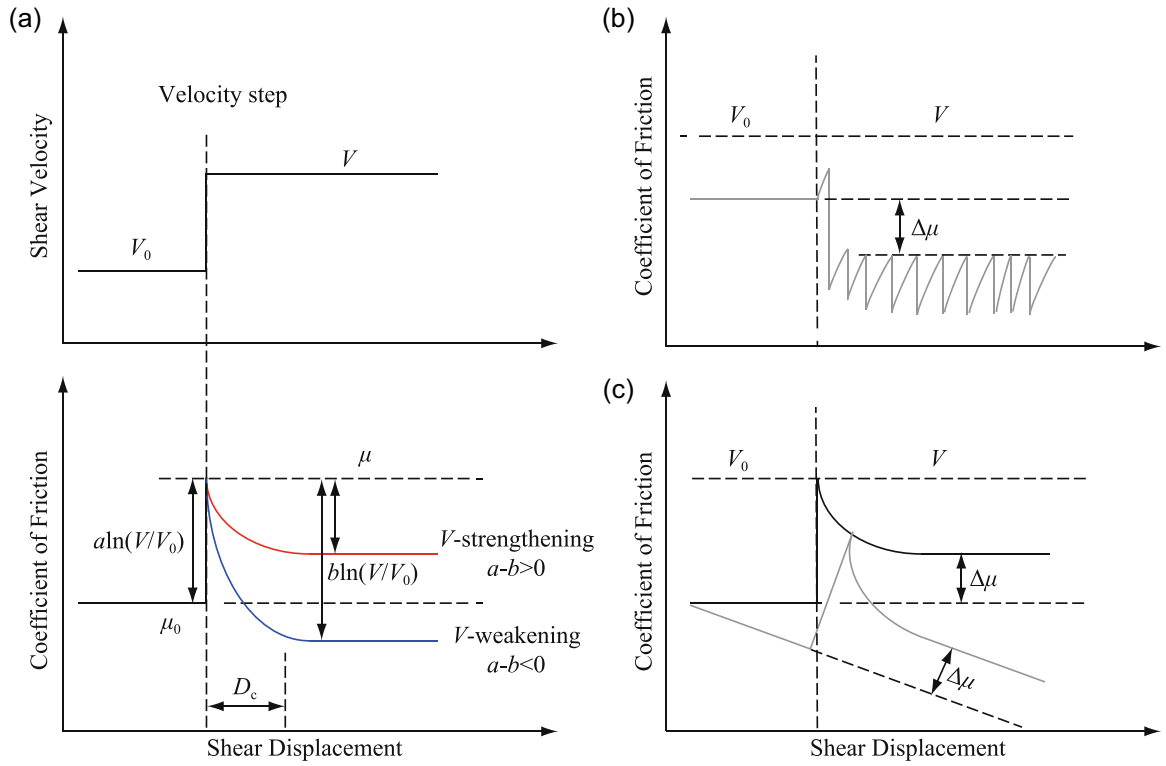

FIGURE 3 Idealized RSF for (a) velocity-strengthening and velocity-weakening responses, and (b) stick-slips. (c) Slope detrending methods in calculating values of $(a-b)$.

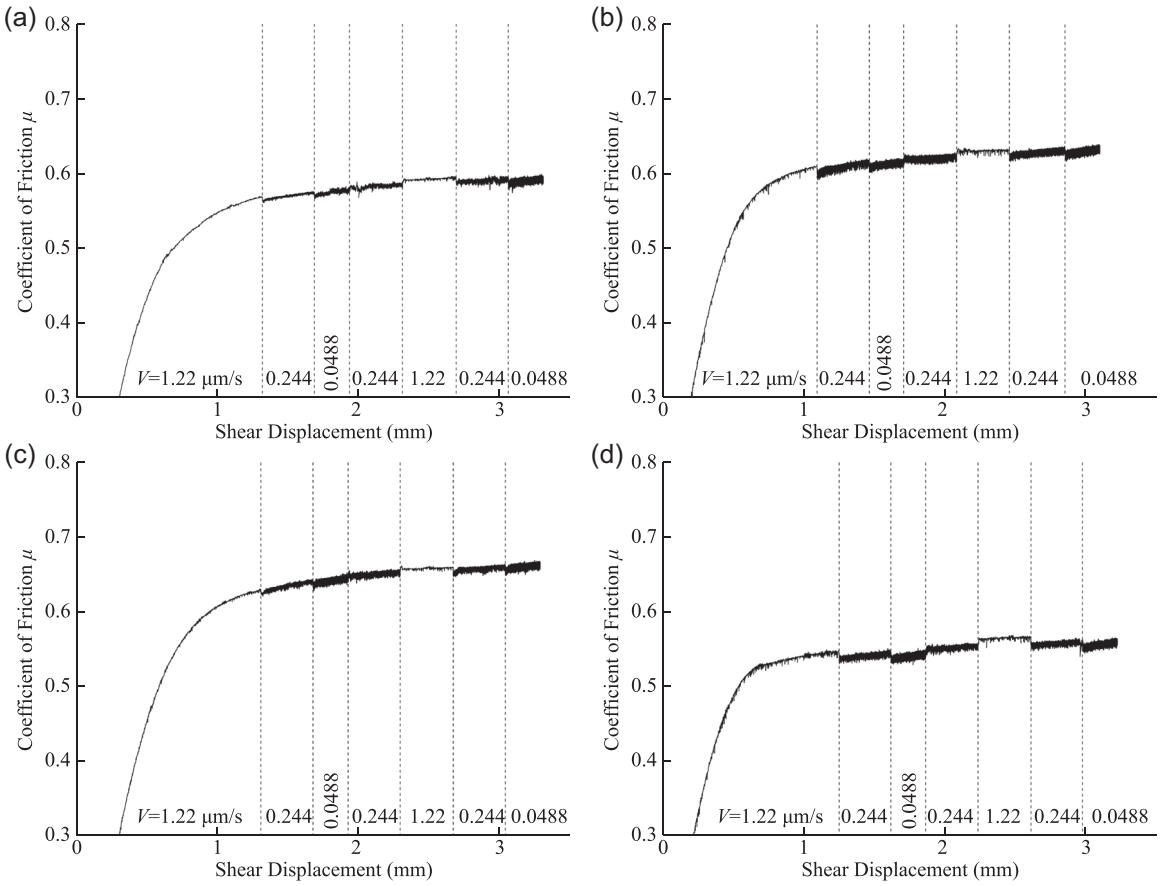

FIGURE 4 Experimental curves showing: (a) SSC3730-2, (b) SSC3740-1, (c) SSC3740-2, and (d) SSC3750 at a confining pressure of 95 MPa, a pore fluid pressure of 40 MPa, and a temperature of 130°C.

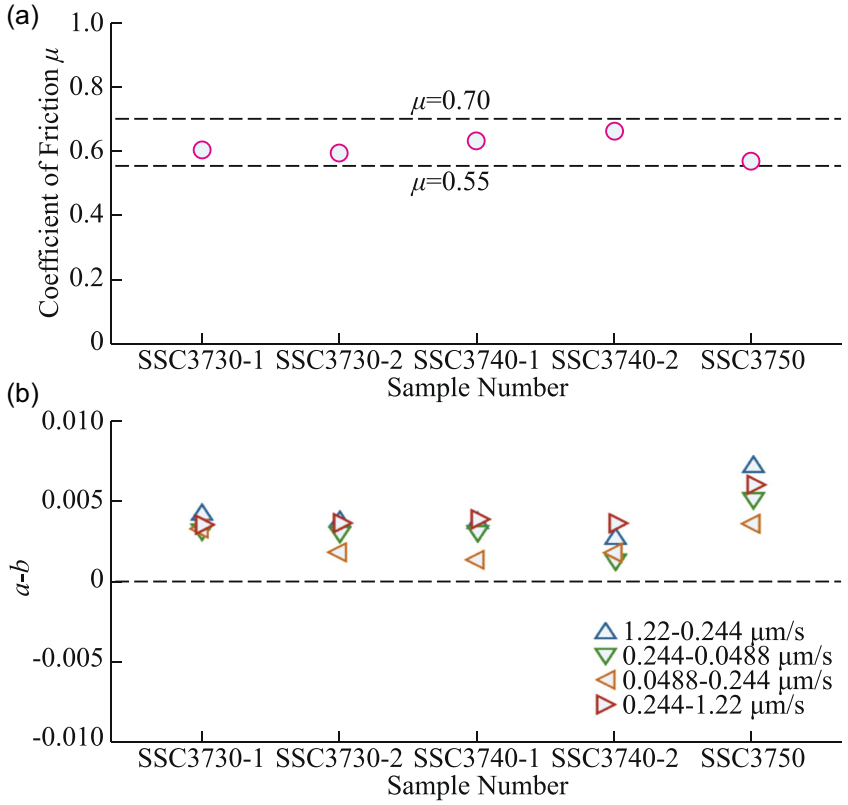

FIGURE 5 Experimental results of μ and $(a-b)$ of samples SSC3730-1, SSC3730-2, SSC3740-1, SSC3740-2, and SSC3750 at a confining pressure of 95 MPa, a pore fluid pressure of 40 MPa, and a temperature of 130°C. The legend indicates the shear velocities. The phyllosilicate contents for samples SSC3730-1, SSC3730-2, SSC3740-1, SSC3740-2, and SSC3750 are 29, 21, 4, 4, and 35 wt.%, respectively. (a) coefficient of friction, (b) frictional stability.

TABLE 3 Results of μ and $(a-b)$ values for all shear experiments

Test No.	Sample No.	μ	$(a-b)$ values at each velocity step (μm/s)			
			1.22–0.244	0.244–0.0488	0.0488–0.244	0.244–1.22
SSC3730-1-90	SSC3730-1	0.616	0.0044	0.0030	0.0033	0.0043
SSC3730-1-130	SSC3730-1	0.601	0.0042	0.0032	0.0033	0.0035
SSC3730-1-200	SSC3730-1	0.609	0.0031	0.0008	0.0009	0.0023
SSC3730-1-270	SSC3730-1	0.669	−0.0060	−0.0010	−0.0006	−0.0046
SSC3730-2-130	SSC3730-2	0.592	0.0037	0.0031	0.0018	0.0036
SSC3740-1-130	SSC3740-1	0.632	0.0037	0.0031	0.0014	0.0039
SSC3740-2-25	SSC3740-2	0.670	−0.0003	−0.0029	0.0007	−0.0007
SSC3740-2-130	SSC3740-2	0.659	0.0027	0.0014	0.0018	0.0036
SSC3740-2-40	SSC3740-2	0.673	−0.0013	−0.0024	−0.0001	−0.0009
SSC3740-2-55	SSC3740-2	0.690	−0.0005	−0.0011	−0.0008	−0.0002
SSC3750-130	SSC3750	0.567	0.0071	0.0052	0.0036	0.0060

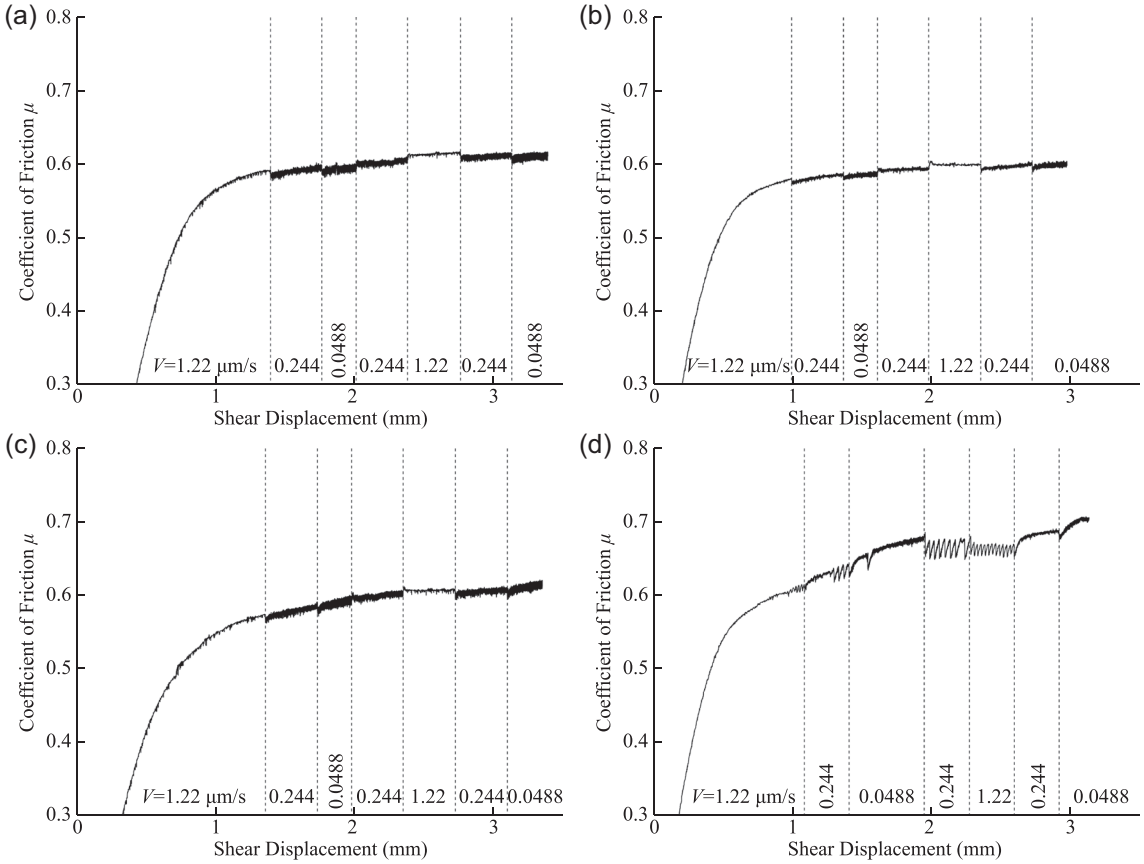

FIGURE 6 Experimental curves showing the gouge SSC3730-1 at a confining pressure of 95 MPa, a pore fluid pressure of 40 MPa, and temperatures of (a) 90°C, (b) 130°C, (c) 200°C, and (d) 270°C, respectively.

following experimental conditions: $\sigma_c = 95$ MPa, $P_f = 40$ MPa, and $T = 90$, 130, 200, and 270°C. The coefficient of friction–shear displacement curves are shown in Figure 6. At $T = 90$°C, 130°C, and 200°C, the gouge SSC3730-1 showed only stable sliding, but stick-slip could be observed at $T = 270$°C. The coefficients of friction (μ) at different temperatures were in the range ~0.60–0.67 (Figure 7a), which indicates that the frictional strength of the studied shale gouge is slightly affected by the temperature at $T \leq 270$°C. With an increase in temperature, the shale gouge SSC3730-1 experienced the transition from velocity-strengthening behavior at $T = 90$°C ($a-b = 0.0027$–0.0043), to velocity-neutral behavior at $T = 200$°C ($a-b = 0.0007$–0.0023), and then velocity-weakening behavior at $T = 270$°C ($a-b = -0.0006$ to -0.0120) (Figure 7b and Table 3).

3.3 | Impact of effective stress on shale gouge friction

Three shear experiments were conducted on the shale gouge SSC3740-2 at $\sigma_c = 95$ MPa, $T = 200$°C, and pore fluid pressures of 25, 40, and 55 MPa to examine the stress dependence of friction and stability. The coefficient of friction–shear displacement curves are shown in Figure 8. At $T = 200$°C, the frictional coefficient slightly rose from 0.67 to 0.69 when the pore fluid pressure was raised from 25 to 55 MPa, showing that the effective stress variation exerts only a minor impact on gouge frictional strength (Figure 9a). As pore fluid pressure rose, the gouge frictional stability also increased slightly, especially at 0.244 – 0.0488 μm/s, indicating that varying the pore fluid pressure also has a minor impact on shale gouge stability (Figure 9b).

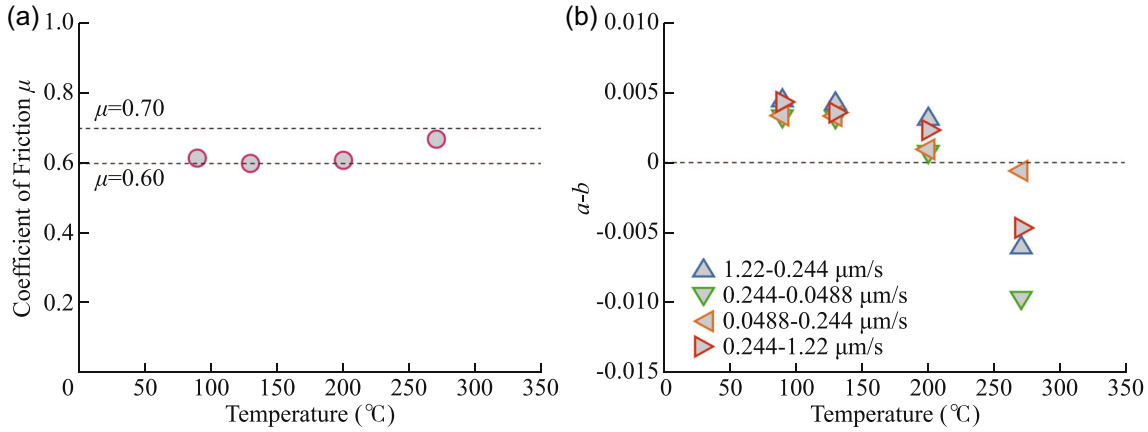

FIGURE 7 Experimental results of μ and $(a - b)$ of the shale gouge SSC3730-1 at a confining pressure of 95 MPa, a pore fluid pressure of 40 MPa, and different temperatures. The legend shows the shear velocities. (a) coefficient of friction, (b) frictional stability.

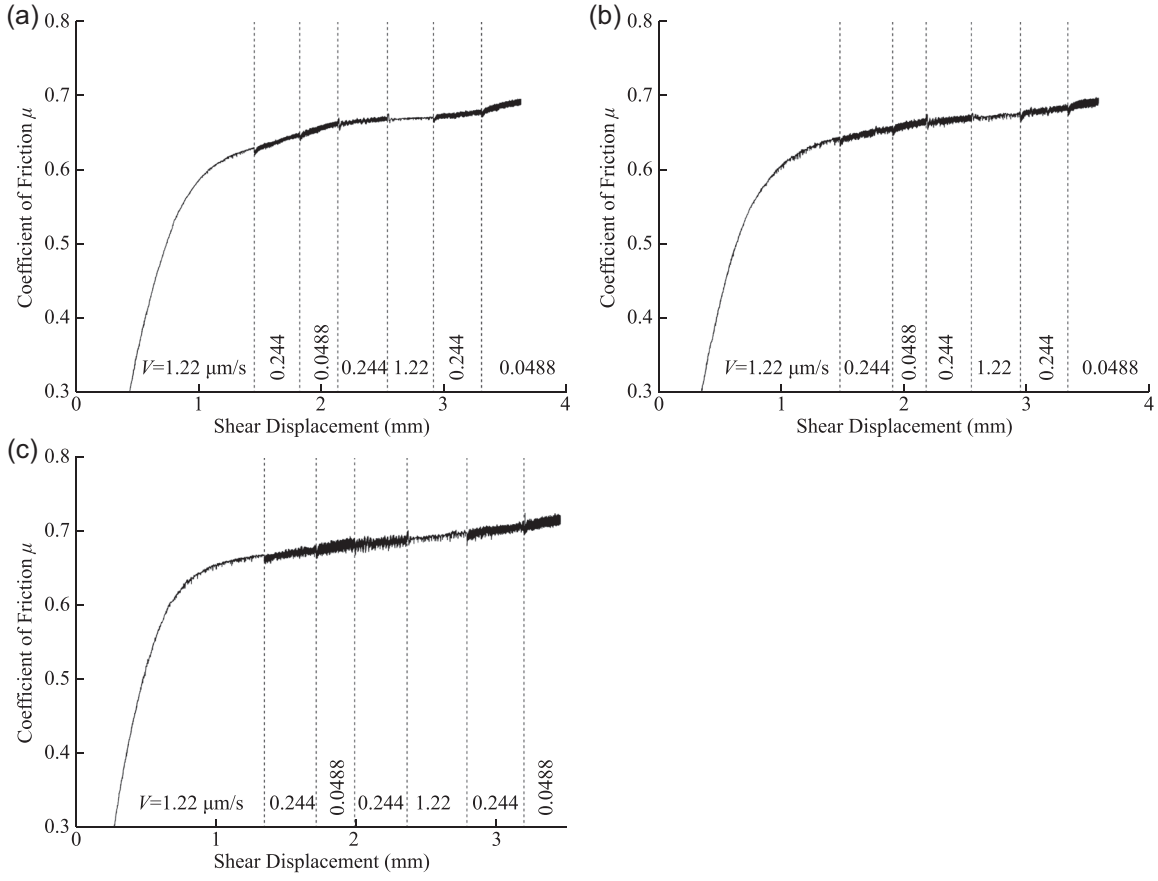

FIGURE 8 Experimental curves showing the gouge SSC3740-2 at a confining pressure of 95 MPa, a temperature of 200°C, and pore fluid pressures of (a) 25 MPa, (b) 40 MPa, and (c) 55 MPa.

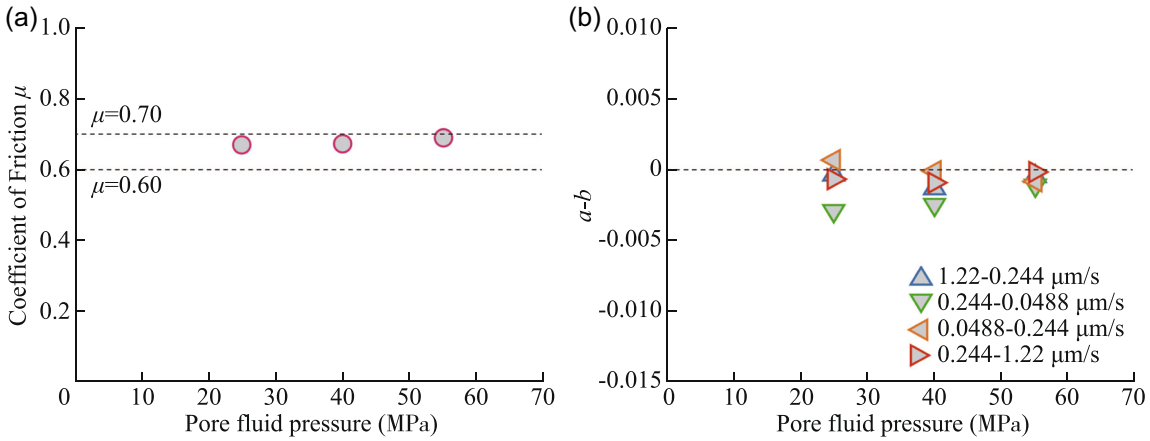

FIGURE 9 Experimental results of μ and $(a-b)$ of the shale gouge SSC3740-2 at a confining pressure of 95 MPa, a temperature of 200°C, and pore fluid pressures of 25, 40, and 55 MPa. The legend shows the shear velocities. (a) coefficient of friction, (b) frictional stability.

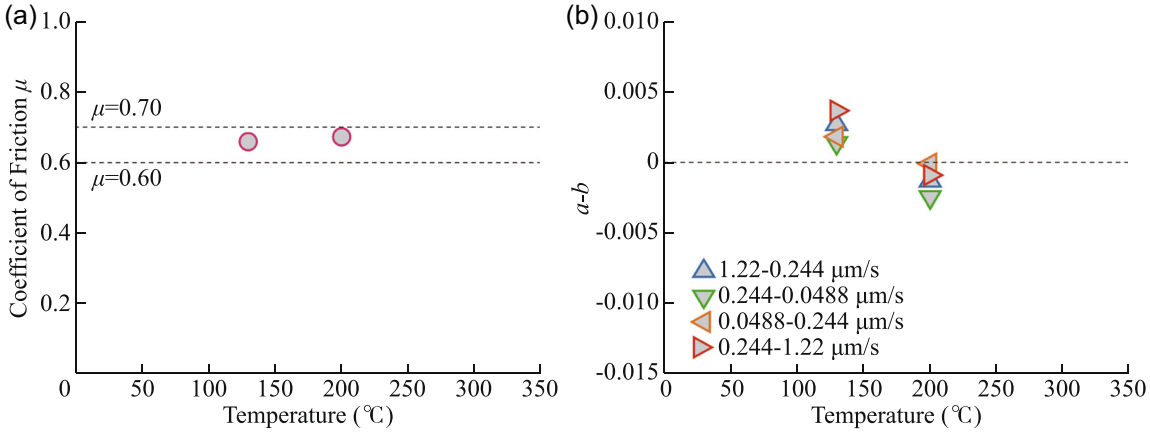

FIGURE 10 Experimental results of (a) coefficient of friction μ and (b) frictional stability $(a-b)$ of the shale gouge SSC3740-2 at a confining pressure of 95 MPa, a pore fluid pressure of 40 MPa, and temperatures of 130°C and 200°C. The legend shows the shear velocities.

4 | DISCUSSION

4.1 | Dependence of shale gouge friction on temperature and mineral composition

The depth of the Longmaxi formation shales varies widely in the southern Sichuan Basin and the Longmaxi formation, therefore, covers a wide range of temperature conditions. From our experimental results, the temperature can affect both the frictional coefficient (μ) and stability ($a-b$) of shale gouges. Four experiments on the shale gouge SSC3730-1 conducted at $\sigma_c = 95$ MPa, $P_f = 40$ MPa, and $T = 90$–270°C exhibit two kinds of velocity dependence. It is characterized by velocity-strengthening behavior ($a-b>0$) at $T = 90$–200°C and a velocity-weakening behavior ($a-b<0$) at $T = 270$°C (Figure 7b). Meanwhile, this stability is accompanied by a slight increase in frictional coefficient. This temperature dependence of gouge friction and stability is generally consistent with previous results on phyllosilicate-bearing gouge (Den Hartog et al., 2012) (Figure 10).

The variation of the gouge frictional stability with temperature can be partially clarified by a microphysical model for phyllosilicate-quartz-dominated gouge (Den Hartog & Spiers, 2014; Niemeijer & Spiers, 2007). In this model, the changes in frictional stability with temperature are caused by the competition between thermally activated gouge compaction and shear-induced dilation. At higher temperatures ($T = 270$°C), the gouge compaction is strong due to the pressure solution and this leads to the compaction dominating the gouge deformation at an upward velocity step. As a consequence, the coefficient of friction would be reduced (Samuelson et al., 2009) and contributes to the observed velocity-weakening behavior. On the contrary, at lower temperatures ($T = 90$–200°C), the gouge dilation dominated the gouge deformation upon an upward velocity step. This leads to an increased coefficient of friction and the observed velocity-strengthening behavior.

The mineral compositions in shales can mainly be divided into three groups, namely, tectosilicates, carbonates, and phyllosilicates. Tectosilicate or carbonate-rich gouges are prone to promote fault instability. Compared with the gouge SSC3730-1, the gouge SSC3740-2 at increasing temperatures exhibits a higher coefficient of friction (μ) and an earlier emergence of negative

frictional stability ($a - b$). This phenomenon is closely related to the mineral composition of two shale gouges. The gouge SSC3740-2 shows a higher tectosilicate content but a lower phyllosilicate content than the gouge SSC3730-1. Compared with many previous research works (An, Zhang, Chen, et al., 2020; Chen et al., 2015; Fang et al., 2018; Kohli & Zoback, 2013), the mineral compositions are shown to be an important factor for shale fault stability.

4.2 | Implications for shale gas recovery

According to previous studies, seismicity associated with hydraulic fracturing during shale gas recovery is closely related to the reactivation of pre-existing faults (An, Zhang, Chen, et al., 2020; Igonin et al., 2021). The results obtained in this study are of great significance for exploring the frictional response of deep faults in shale reservoirs of the southeastern Sichuan Basin. The experimental results show that the fault frictional properties are influenced by the temperature and mineral compositions during hydraulic fracturing. Since the depth of current hydraulic fracturing is generally shallower than 3.5 km, the in situ temperature in these reservoirs should be less than 150°C (Ma & Xie, 2018). According to our experimental results, most shale fault slips in these shallow reservoirs should be aseismic. However, three earthquakes with Mw ≥ 4.7 have been detected in this area (2017–2019), which have been proven to be closely associated with hydraulic fracturing (Wang et al., 2022). This manifests the possibility of moderate earthquakes in shallow shale reservoirs. With the shale gas exploitation toward a deeper depth in the southeastern Sichuan Basin (Xu et al., 2019; C. Zou et al., 2015), the temperature would be much higher than the shallow reservoirs and thus the seismic hazard would also be increased in deeper reservoirs.

The magnitude and number of seismic events are closely related to the reservoir temperature. From the experimental results, the frictional instability of shale gouges is enhanced with an increase in reservoir temperature, indicating that the seismic hazard also increases at higher temperatures. The burial depths of the Longmaxi formation are generally in the range of 1.5–5 km in the southern Sichuan Basin, with corresponding in situ temperatures in the range of 50–180°C. As the depth of the target reservoir increases, the potential for fault instability and hazard of induced seismicity will increase dramatically. Although temperature is not the main factor controlling seismicity in the shallow shale reservoirs (An, Zhang, Chen, et al., 2020), the high temperature can impact the fault stability in deep shale reservoirs. Additionally, the mineral composition of the deep Longmaxi shale reservoir varies significantly and may also favor velocity-weakening behavior at increased depths. From Figure 5b, it can be seen that the mineral composition changes significantly with the change in burial depth and this change exerts a strong control on frictional stability. Therefore, the combined effect of temperature and mineral composition is particularly important for the occurrence of seismic activities at deep shale reservoirs.

5 | CONCLUSIONS

We explored the effects of the variations in mineral composition, temperature, and effective stress on the frictional and stability properties of Longmaxi shale gouges at depths that are representative of the southeastern Sichuan Basin, southwest China. The mineral compositions of the collected shales were analyzed and the shear experiments were performed under hydrothermal conditions. The mineral compositions in five Longmaxi shales from the Luzhou block mainly include quartz, plagioclase, calcite, dolomite, and clay minerals (mainly illite and chlorite) and vary with increasing depth. Both the mineral composition and temperature can impact the frictional coefficient and stability of Longmaxi shale gouges, while the effective stress variation only exerts a minor control. The frictional strengths increase with increasing tectosilicate and carbonate contents and the gouge instability is also enhanced at higher tectosilicate and carbonate contents. With the increasing temperature, the frictional strength of shale gouges increases slightly. However, a transition from velocity-strengthening to velocity-weakening behavior is identified at a threshold of temperature of 200°C. The combined effect of temperature and mineral composition is important for controlling the shale fault frictional response, especially for the deeper shale reservoirs in the southeastern Sichuan Basin.

ACKNOWLEDGMENTS

This research is funded by the National Natural Science Foundation of China (42077247 and 42107163), the China Postdoctoral Science Foundation (2021M692448 and 2022T150483), and the Fundamental Research Funds for the Central Universities. We appreciate the assistance of Wenming Yao and Jianye Chen in the lab.

CONFLICT OF INTEREST

The authors declare no conflict of interest.

DATA AVAILABILITY STATEMENT

The data that support the findings of this study are available from the corresponding author upon reasonable request.

ETHICS STATEMENT

There are no ethical issues with this study.

REFERENCES

An M, Zhang F, Chen Z, Elsworth D, Zhang L. Temperature and fluid pressurization effects on frictional stability of shale faults reactivated by hydraulic fracturing in the Changning block, southwest China. *J Geophys Res*. 2020;125:e2020JB019584. doi:10.1029/2020JB019584

An M, Zhang F, Elsworth D, Xu Z, Chen Z, Zhang L. Friction of Longmaxi shale gouges and implications for seismicity during hydraulic fracturing. *J Geophys Res*. 2020;125:e2020JB019885. doi:10.1029/2020JB019885

Atkinson GM, Eaton DW, Igonin N. Developments in understanding seismicity triggered by hydraulic fracturing. *Nat Rev Earth Environ*. 2020;1:264-277. doi:10.1038/s43017-020-0049-7

Bao X, Eaton DW. Fault activation by hydraulic fracturing in western Canada. *Science*. 2016;354(6318):1406-1409. doi:10.1126/science.aag2583

Candela T, Brodsky EE, Marone C, Elsworth D. Flow rate dictates permeability enhancement during fluid pressure oscillations in laboratory experiments. *J Geophys Res*. 2015;120:2037-2055. doi:10.1002/2014JB011511

Candela T, Wassing B, Heege J. How earthquake are induced. *Science*. 2018;360(6389):598-600. doi:10.1126/science.aat2776

Cappa F, Rutqvist J. Impact of CO_2 geological sequestration on the nucleation of earthquakes. *Geophys Res Lett*. 2011;38(17):L17313. doi:10.1029/2011GL048487

Chang KW, Yoon H, Kim Y, Lee MY. Operational and geological controls of coupled poroelastic stressing and pore-pressure accumulation along faults: induced earthquakes in Pohang, South Korea. *Scientific Rep*. 2020;10:2073. doi:10.1038/s41598-020-58881-z

Chen J, Verberne BA, Spiers CJ. Interseismic re-strengthening and stabilization of carbonate faults by "non-Dieterich" healing under hydrothermal conditions. *Earth Planet Sci Lett*. 2015;423:1-12. doi:10.1016/j.epsl.2015.03.044

Clarke H, Verdon JP, Kettlety T, Baird AF, Kendall JM. Real time imaging, forecasting and management of human-induced seismicity at Preston New Road, Lancashire, England. *Seismol Res Lett*. 2019;90(5):1902-1915. doi:10.1785/0220190110

Dieterich JH. Time-dependent friction and the mechanics of stick-slip. *Pure Appl Geophys*. 1978;116(4-5):790-806. doi:10.1007/BF00876539

Dieterich JH. Modeling of rock friction: 1. Experimental results and constitutive equations. *J Geophys Res*. 1979;84(B5):2161. doi:10.1029/JB084iB05p02161

Ellsworth WL. Injection-induced earthquakes. *Science*. 2013;341(6142):142-149. doi:10.1126/science.1225942

Elsworth D, Spiers CJ, Niemeijer AR. Understanding induced seismicity. *Science*. 2016;354(6318):1380-1381. doi:10.1126/science.aal2584

Fang Y, den Hartog SAM, Elsworth D, Marone C, Cladouhos T. Anomalous distribution of microearthquakes in the Newberry Geothermal Reservoir: mechanisms and implications. *Geothermics*. 2016;63:62-73. doi:10.1016/j.geothermics.2015.04.005

Fang Y, Elsworth D, Wang C, Ishibashi T, Fitts JP. Frictional stability–permeability relationships for fractures in shales. *J Geophys Res*. 2017;122:1760-1776. doi:10.1002/2016JB01343

Fang Y, Elsworth D, Wang C, Jia Y. Mineralogical controls on frictional strength, stability, and shear permeability evolution of fractures. *J Geophys Res*. 2018;123:3549-3563. doi:10.1029/2017JB015338

Grigoli F, Cesca S, Priolo E, et al. Current challenges in monitoring, discrimination, and management of induced seismicity related to underground industrial activities: a European perspective. *Rev Geophys*. 2017;55:310-340. doi:10.1002/2016RG000542

Grigoli F, Cesca S, Rinaldi AP, et al. The November 2017 Mw 5.5 Pohang earthquake: a possible case of induced seismicity in South Korea. *Science*. 2018;360(6392):1003-1006. doi:10.1126/science.aat2010

Guglielmi Y, Elsworth D, Cappa F, et al. In situ observations on the coupling between hydraulic diffusivity and displacements during fault reactivation in shales. *J Geophys Res*. 2015;120:7729-7748. doi:10.1002/2015JB012158

Den Hartog SAM, Niemeijer AR, Spiers CJ. New constraints on megathrust slip stability under subduction zone P–T conditions. *Earth Planet Sci Lett*. 2012;353-354:240-252. doi:10.1016/j.epsl.2012.08.022

Den Hartog SAM, Spiers CJ. A microphysical model for fault gouge friction applied to subduction megathrusts. *J Geophys Res*. 2014;119:1510-1529. doi:10.1002/2013JB010580

He C, Yao W, Wang Z, Zhou Y. Strength and stability of frictional sliding of gabbro gouge at elevated temperatures. *Tectonophysics*. 2006;427(1-4):217-229. doi:10.1016/j.tecto.2006.05.023

Igonin N, Verdon JP, Kendall J-M, Eaton DW. Largescale fracture systems are permeable pathways for fault activation during hydraulic fracturing. *J Geophys Res*. 2021;126:e2020JB020311. doi:10.1029/2020JB020311

Ikari MJ, Marone C, Saffer DM. On the relation between fault strength and frictional stability. *Geology*. 2011;39(1):83-86. doi:10.1130/G31416.1

Jia Y, Fang Y, Elsworth D, Wu W. Slip velocity dependence of friction-permeability response of shale fractures. *Rock Mech Rock Eng*. 2019;53(5):2109-2121. doi:10.1007/s00603-019-02036-8

Juanes R, Jha B, Hager BH, et al. Were the May 2012 Emilia-Romagna earthquakes induced? A coupled flow-geomechanics modeling assessment. *Geophys Res Lett*. 2016;43(13):6891-6897. doi:10.1002/2016GL069284

Kohli AH, Zoback MD. Frictional properties of shale reservoir rocks. *J Geophys Res*. 2013;118(9):5109-5125. doi:10.1002/jgrb.50346

Lei X, Huang D, Su J, et al. Fault reactivation and earthquakes with magnitudes of up to Mw4. 7 induced by shale-gas hydraulic fracturing in Sichuan Basin, China. *Scientific Rep*. 2017;7:7971. doi:10.1038/s41598-017-08557-y

Lei X, Su J, Wang Z. Growing seismicity in the Sichuan Basin and its association with industrial activities. *Sci China Earth Sci*. 2020;63:1-28. doi:10.1007/s11430-020-9646-x

Lei X, Wang Z, Su J. Possible link between long-term and short-term water injections and earthquakes in salt mine and shale gas site in Changning, south Sichuan Basin, China. *Earth Planet Phys*. 2019a;3:510-525. doi:10.26464/epp2019052

Lei X, Wang Z, Su J. The December 2018 M_L 5.7 and January 2019 M_L 5.3 earthquakes in South Sichuan Basin induced by shale gas hydraulic fracturing. *Seismol Res Lett*. 2019b;90(3):1099-1110. doi:10.1785/0220190029

López-Comino JA, Cesca S. Source complexity of an injection induced event: the 2016 Mw 5.1 Fairview, Oklahoma earthquake. *Geophys Res Lett*. 2018;45:4025-4032. doi:10.1029/2018GL077631

Ma X. Enrichment laws and scale effective development of shale gas in the southern Sichuan Basin. *Nat Gas Ind B*. 2018;38(10):1-10.

Ma X, Xie J. The progress and prospects of shale gas exploration and exploitation in southern Sichuan Basin, NW China. *Pet Explor Dev*. 2018;45(1):161-169.

Marone C. Laboratory-derived friction laws and their application to seismic faulting. *Annu Rev Earth Planet Sci*. 1998;26(1):643-696. doi:10.1146/annurev.earth.26.1.643

Niemeijer AR, Spiers CJ. A microphysical model for strong velocity weakening in phyllosilicate-bearing fault gouges. *J Geophys Res*. 2007;112:B10405. doi:10.1029/2007JB005008

Ruina A. Slip instability and state variable friction laws. *J Geophys Res*. 1983;88(B12):10359-10370. doi:10.1029/JB088iB12p10359

Samuelson J, Elsworth D, Marone C. Shear-induced dilatancy of fluid-saturated faults: experiment and theory. *J Geophys Res*. 2009;114:B12404. doi:10.1029/2008JB006273

Schultz R, Skoumal RJ, Brudzinski MR, Eaton D, Baptie B, Ellsworth W. Hydraulic fracturing-induced seismicity. *Rev Geophys*. 2020;58(3):e2019RG000695. doi:10.1029/2019RG000695

Scuderi MM, Collettini C. The role of fluid pressure in induced vs. triggered seismicity: insights from rock deformation experiments on carbonates. *Scientific Rep*. 2016;6:24852. doi:10.1038/srep24852

Scuderi MM, Collettini C. Fluid injection and the mechanics of frictional stability of shale-bearing faults. *J Geophys Res*. 2018;123(10):8364-8384. doi:10.1029/2018JB016084

Segall P, Lu S. Injection-induced seismicity: poroelastic and earthquake nucleation effects. *J Geophys Res*. 2015;120(7):5082-5103. doi:10.1002/2015JB012060

Verdon JP, Bommer J. Green, yellow, red, or out of the blue? An assessment of Traffic Light Schemes to mitigate the impact of hydraulic fracturing-induced seismicity. *J Seismol*. 2020;24(5):1-26. doi:10.1007/s10950-020-09966-9

Wang S, Jiang G, Lei X, et al. Three Mw ≥ 4.7 earthquakes within the Changning (China) shale gas field ruptured shallow faults intersecting with hydraulic fracturing wells. *J Geophys Res*. 2022;127(2):e2021JB022946. doi:10.1029/2021JB022946

Xu Z, Jiang S, Yao G, Liang X, Xiong S. Tectonic and depositional setting of the lower Cambrian and lower Silurian marine shales in the Yangtze Platform, South China: implications for shale gas exploration and production. *J. Asian Earth Sci*. 2019;170:1-19. doi:10.1016/j.jseaes.2018.10.023

Yasuhara H, Elsworth D, Polak A. Evolution of permeability in a natural fracture: significant role of pressure solution. *J Geophys Res*. 2004;109(B3):B03204. doi:10.1029/2003jb002663

Yasuhara H, Marone C, Elsworth D. Fault zone restrengthening and frictional healing: the role of pressure solution. *J Geophys Res*. 2005;110:B06310. doi:10.1029/2004jb003327

Zhang F, An M, Zhang L, Fang Y, Elsworth D. The role of mineral composition on the frictional and stability properties of powdered reservoir rocks. *J Geophys Res*. 2019;124:1480-1497. doi:10.1029/2018JB016174

Zhang F, Fang Y, Elsworth D, Wang C, Yang X. Evolution of friction and permeability in a propped fracture under shear. *Geofluids*. 2017;2017:2063747. doi:10.1155/2017/2063747

Zhang L, He C. Frictional properties of phyllosilicate-rich mylonite and conditions for the brittle-ductile transition. *J Geophys Res*. 2016;121:3017-3047. doi:10.1002/2015JB012489

Zou C, Dong D, Wang Y, et al. Shale gas in China: characteristics, challenges and prospects (I). *Pet Explor Dev*. 2015;42(6):689-701.

Zou X, Li X, Wang Y, Zhang J, Zhao P. Reservoir characteristics and gas content of Wufeng–Longmaxi formations deep shale in southern Sichuan Basin. *Nat Gas Geosci*. 2022;33(4):654-665. (in Chinese with an English abstract).

AUTHOR BIOGRAPHY

Mengke An is a postdoctor at the Department of Geotechnical Engineering of Tongji University since 2021. He received his Ph.D. in Civil Engineering from Tongji University in 2020 and a B.Sc. in Civil Engineering from China University of Geosciences, Beijing in 2015. His research interests are in the multifield coupling in rock mechanics and the deep fault stability applied to shale gas recovery, enhanced geothermal system, carbon dioxide sequestration, and lunar exploration. Current efforts are focused on understanding the mechanisms of mineral alteration in shallow geothermal reservoirs, the effect of metamorphosed minerals on granite fault stability, and the stability mechanisms of lunar regolith and fractured crust.

How to cite this article: Zhang F, Cui L, An M, Elsworth D, He C. Frictional stability of Longmaxi shale gouges and its implication for deep seismic potential in the southeastern Sichuan Basin. *Deep Undergr Sci Eng*. 2022;1-12. doi:10.1002/dug2.12013